Sizes of Multilamellar Vesicles in Shear

C.-Y. David Lu*

Department of Chemistry and Department of Physics, Center of Theoretical Physics, National Taiwan University, Taipei 106, Taiwan

(Received 10 May 2012; published 19 September 2012)

The dynamics of the multilamellar vesicle (MLV) is analyzed theoretically, where membrane interaction squeezes the solvent to flow between the neighboring membranes. With the applied affine shear, the dynamic free energy density of the MLV develops a minima, which selects the MLV size. The model predicts a terminal shear rate, below which the metastable MLV exists. The scaling relations for the MLV size and the terminal shear are both consistent with the experiments.

DOI: 10.1103/PhysRevLett.109.128304 PACS numbers: 82.70.Uv, 64.70.mf, 83.60.Rs, 87.16.D−

Multilamellar vesicles (MLVs) have an onionlike structure, where the concentric bilayer vesicles are nested to form a multilayer vesicle. Its space-dividing structure leads to many applications, for example, the microreactor [1] or the container for smooth drug release processes [2]. Such MLV structures can arise as a thermodynamic stable phase [3,4], where the space is packed delicately by polydisperse MLVs to reduce their deformation. Alternatively, metastable MLVs can be produced from lamellar phases by external forcing. Several methods have been reported to produce metastable MLVs, including the dry lipid hydration, the sonication method [5], the electrode method, and the flow method. While a simple pressure-driven flow through narrow pores can generate MLVs, uniform shear flows, surprisingly, have been reported to induce a sharp transition from the lamellar phase to MLVs [6–11], where the (metastable) MLVs have a monodisperse size distribution. The shear flow method is successfully applied to both surfactant solutions and copolymer-homopolymer mixtures [12,13], and so it seems to be a generic phenomena.

The shear flow—induced transition process has such a narrow MLV size distribution that it has generated a lot of interest in understanding its mechanism. Theoretical studies [14–16] show that as the shear rate gradually increases, the lamellar will lose its stability, and either the direction or the layer fluctuation will be affected by shear. At much higher shear rates, stability analysis [17] shows that the undulation instability along the velocity direction will disappear, and the lamellar will become stable again. Therefore, in the intermediate shear rates, the unstable lamellar reorganizes itself into nontrivial structures. Scattering experiments reveal that the unstable lamellar first organizes itself into multilayer cylinders, which later become the MLVs as the steady state [18,19].

To understand the relation between the MLV size and the steady-state shear rate, many theories have been inspired by the oil droplet breakup problem pioneered by Taylor [6,20–23]. In shear flow, small droplets merge, and the droplet will break if the viscous force on it is stronger than the elastic force. When the droplets reach their steady-state size, one can obtain the scaling relation for the droplet size by balancing the viscous force with the elastic force. In the oil-water system, the elastic force comes from the surface tension and the curvature. For the MLVs, the static calculation of a slightly deformed MLV [24] suggests that an effective surface tension can be defined. Using the effective surface tension, Taylor's argument can be applied, which gives the MLV size—shear rate scaling relation [6,21–23]. Since the general idea is not specific enough, several different theories exist.

In an early review of shear-induced MLVs [11], Richtering pointed out that all the reported cases are multicomponent (lyotropic) systems. Furthermore, Kato *et al.* [25] found that when the amount of the solvent is too small, MLVs do not form. We believe that the multicomponent feature is significant. The force balance picture mentioned above, however, does not distinguish single- or multicomponent smectics.

Compared with single-component smectics, multicomponent smectics have at least one more hydrodynamic slow mode, arising from the additional conservation law of the second component [26]. In the surfactant system where MLVs form, this mode has the slowest relaxation rate. The decay rate was calculated by Brochard and de Gennes [27] (called the "slip mode"), and measured by dynamic scattering [26] (as the "baroclinic mode"). MLVs have finite sizes; therefore, this mode is no longer hydrodynamic in the strict sense. Nonetheless, its slow rate suggests that it may have an important role to play in the mechanism of MLV formation.

In this Letter, we study the slow mode of a MLV, using a model similar to that in Ref. [28] for the flat lamellar. When a shear is applied, we find that the dynamic free energy density develops a minima, which selects the MLV size. We are able to derive detailed scaling prediction for the MLV size, where the dependence on the smectic repeat distance d is included. The predicted MLV size has the correct scalings with the shear rate and concentration. Above a terminal shear rate, the minima disappears, indicating that the MLV becomes unstable. Our terminal shear rate expression is also consistent with the experimental phase boundary. These suggest that the slow mode is essential for the formation of MLVs.

We consider a MLV consisting of N nested bilayer vesicles. The bilayer thickness is assumed to be small. The equilibrium surface of the nth layer (with $1 \leq n \leq N$) is a sphere with radius $r_n = nd$. To describe the relaxation of small fluctuations, we introduce the layer normal displacement u_n of the nth layer, and its dimensionless surface concentration ϕ_n, which becomes unity at equilibrium. We use the free energy [27,29]

$$F = \int^{r_N} dr \int dA \frac{\bar{B}(\partial_r u)^2}{2} + \sum_{n=1}^{N} \int dA \left(\frac{\kappa}{2} H_n^2 + \frac{E_S(\phi_n - 1)^2}{2} \right) \quad (1)$$

where $H_n = 2/r_n - (\hat{L}^2 u_n)/r_n^2$ is (twice) the mean curvature of the bilayer; $\hat{L}^2$ is the angular momentum operator without $\hbar$. The quantities u_n, H_n, and ϕ_n are functions of the polar angles θ, φ. The first term describes the interaction between the neighboring layers, where $\bar{B}$ is the compression modulus. The second term gives the bending energy [29]. The third term gives the stretching energy [29] from the surface concentration variation. For simplicity, the small coupling between the surface concentration and the layer dilation is neglected [26,30]. Note that we use the surface concentration as the dynamic variable, instead of the concentration. The large stretching modulus ensures a fast-relaxing surface concentration. Therefore ϕ_n is more suitable for the adiabatic approximation [31].

The solvent surrounding the bilayers is described by the Stokes equation, with the solvent viscosity η

$$-\nabla p + \eta \nabla^2 \mathbf{v} = 0, \quad (2)$$

and the incompressible constraint $\nabla \cdot \mathbf{v} = 0$. At the bilayers, we assume the nonslip boundary condition.

We neglect the solvent permeation through the bilayers. For the radial velocity at r_n, we write

$$\partial_t u_n + \mathbf{v}_\perp \cdot \nabla_\perp u_n = v_r \quad (3)$$

The dynamical equation for surface concentration is

$$\partial_t \phi_n + \mathbf{v}_\perp \cdot \nabla_\perp \phi_n = -\frac{2v_r}{r_n} \phi_n - (\nabla_\perp \cdot \mathbf{v}_\perp)\phi_n \quad (4)$$

The sum of the forces on each bilayer vanishes. The normal force balance reads

$$-\frac{\delta F}{\delta u_n} + \sigma_{rr}(r_n^+) - \sigma_{rr}(r_n^-) = 0 \quad (5)$$

where $\sigma_{rr} = -p + 2\eta \partial_r v_r$, and $r_n^\pm = \lim_{\epsilon \to 0} r_n \pm |\epsilon|$.

The tangential force balance on the bilayer is

$$-\frac{\delta F}{\delta \mathbf{x}_n} + \sigma_{r\perp}(r_n^+) - \sigma_{r\perp}(r_n^-) = 0 \quad (6)$$

where $\mathbf{x}_n$ is the tangential (2D) displacement vector. The (2D) stress $\sigma_{r\perp}$ has the standard stress components.

For the boundary conditions, in this study, we consider the MLV to be densely packed with its neighbors. In the spherical unit cell approximation, the boundary is a spherical cell with radius $r_N + d$.

We first consider the relaxation shape without the external shear. The homogeneous Eq. (5) can be put into a matrix form in N dimension

$$\mathbf{E} \cdot \mathbf{u} + \mathbf{R} \cdot \partial_t \mathbf{u} = 0 \quad (7)$$

where $\mathbf{u} = (u_1, \ldots, u_N)$. The matrix $\mathbf{E}$ contains the bending force and the $\bar{B}$ term. The stretching force and the stress σ_{rr} consist of the matrix $\mathbf{R}$. We consider the limit of the large stretching modulus, $E_S \to \infty$ (hence $\phi_n \to 1$), so that Eq. (4) becomes the surface incompressibility condition $2v_r/r_n + \nabla_\perp \cdot \mathbf{v}_\perp = 0$. The flow field obeys three constraints, that of bulk incompressibility, and of surface incompressibility at the two surfaces r_{n-1} and r_n. The Poiseuille flow between the two neighboring layers is fully determined by the layer normal velocities $v_r(r_{n-1}) = \partial_t u_{n-1}$ and $v_r(r_n) = \partial_t u_n$. Stress components can be calculated from the fluid velocity and pressure. The stretching force becomes a Lagrange multiplier, which is determined from $\sigma_{r\perp}$ through Eq. (6).

The relaxation spectrum resembles that of the flat smectics. As shown in Fig. 1, the numerical decay rates agree with the baroclinic mode dispersion relation

$$\Gamma_b = \mu \bar{B} \frac{l(l+1)}{r_n^2} \quad (8)$$

where $\mu = d^2/12\eta$ is the Brochard–de Gennes mobility for the "slip mode" [27]. The baroclinic mode dispersion is very accurate except for the high-frequency modes near the center of the MLV, where the modes acquire the undulation character. At low l, the relaxation modes are predominant baroclinic modes. One can note that, at $l = 2$, the decay rate Γ_b for r_N is very close to the MLV formation shear rate [32]. This suggests that the MLV size might be limited by the criterion that all the internal relaxations must be faster than the applied shear rate.

We now consider the MLV with the external shear flow. The velocity of a simple shear is $\mathbf{v} = \kappa_s \cdot \mathbf{r}$. The velocity

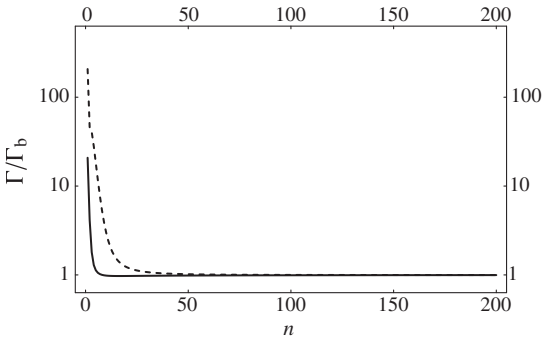

FIG. 1. The ratio of the numerical relaxation rates Γ and the approximated expression Γ_b. For the majority of the slow modes, $\Gamma = \Gamma_b$. The solid line has $l = 2$. The dashed line is for $l = 8$. Both curves have $\lambda/d = 1.9$ and $N = 200$.

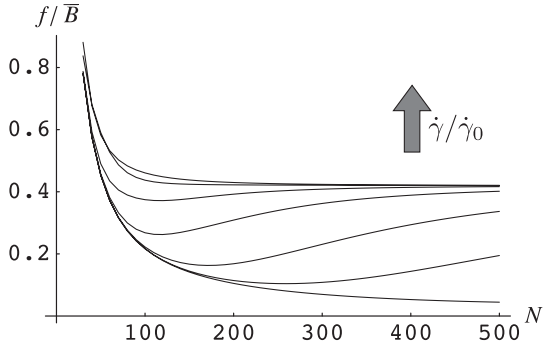

FIG. 2. The dynamic free energy density f for $\lambda/d = 3.65$. From the lowest curve upward, the ratios $\dot{\gamma}_0/\dot{\gamma}$ are 1.87×10^6, 1.87×10^5, 6.2×10^4, 1.87×10^4, 6.2×10^3, 1.87×10^3, and 187. The upper two curves do not have a minima.

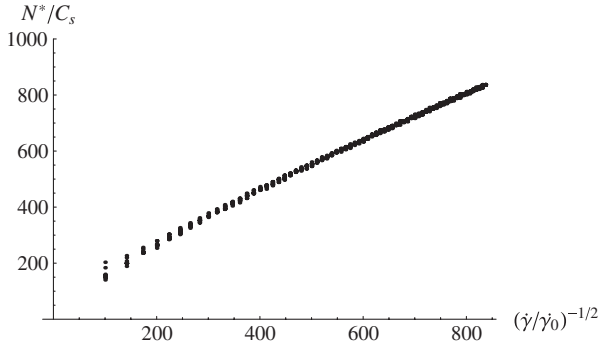

FIG. 3. The size-shear rate relation. The numerical data are from $\lambda/d = 0.125$, 0.25, 0.7, 1.0, 1.5, 2.0, 3.3, and 3.65.

gradient tensor is $\kappa_s = \dot{\gamma}\,\hat{\mathbf{x}}\,\hat{\mathbf{y}}$, where $\hat{\mathbf{x}}$ and $\hat{\mathbf{y}}$ are the unit vectors along the x and y directions.

On a MLV, the torque produced by the applied shear stress must be balanced by other torques. If all the MLVs rotate in the same direction, some neighboring MLVs along the flow direction will shear against each other, so that an opposite torque arises from such shear stress. A detailed calculation is beyond the scope of the present work. Below we will simply assume that the MLV rotates at the rate $\dot{\gamma}$. In the rotating frame corotated with the MLV, the radial velocity becomes

$$v_r(\mathbf{r}, t) = \sqrt{\frac{4\pi}{15}}\dot{\gamma} r (Y_2^x \sin\dot{\gamma}t + Y_2^y \cos\dot{\gamma}t) \tag{9}$$

where $Y_2^x(\theta, \varphi) = \sqrt{45/48\pi}\sin^2\theta\cos 2\varphi$ and $Y_2^y(\theta, \varphi) = \sqrt{45/48\pi}\sin^2\theta\sin 2\varphi$. In the rotating frame, the layer displacement now has the inhomogeneous term

$$\mathbf{E}\cdot\mathbf{u} + \mathbf{R}\cdot\partial_t\mathbf{u} = \mathbf{R}\cdot\mathbf{v_r} \tag{10}$$

where v_r evaluated at r_n forms the N dimension vector $\mathbf{v_r}$. Equation (10) can be put into a dimensionless form, where the shear rate is measured by $\dot{\gamma}_0 \equiv 6\mu\bar{B}/d^2$. The solution depends only on the dimensionless parameter λ/d. Here $\lambda \equiv \sqrt{K/\bar{B}}$ is the smectic penetration length, and $K = \kappa/d$ is the bending modulus. For typical systems, the ratio λ/d is close to unity.

In Fig. 2, we solve Eq. (10) numerically, and use Eq. (1) to evaluate the dynamic free energy density f, defined as

$$f(N, \dot{\gamma}) \equiv \frac{F}{4\pi r_N^3/3} \tag{11}$$

which depends on N and $\dot{\gamma}$. In static or at very small shear rates, the decreasing free energy density agrees with the static calculation (see Ref. [24]), where the shear modulus scales as $\sqrt{K\bar{B}}/r_N$. For a MLV with N layers, at shear rates larger than $6\mu\bar{B}/r_N^2$, some of its slow modes cannot follow the shear rate; therefore, the free energy density increases. For a given shear rate, the large MLVs are affected, while the small MLVs remain the same as static; therefore f develops a minima N^*, representing an optimal MLV size at that shear rate. The optimal size N^* decreases as the shear rate increases. Above a maxima shear rate $\dot{\gamma}_{\max}$, where the optimal MLV size is close to the core size λ, the free energy loses the minima.

In Fig. 3, we find that the numerical data of N^*, scaled by a coefficient C_s, form a scaling relation, where

$$C_s \simeq 0.37(\lambda/d)^{1/4} \tag{12}$$

between $0.25 \le \lambda/d \le 4$ with error below 5%. At low shear rates, we obtain $N^*/C_s \simeq (\dot{\gamma}/\dot{\gamma}_0)^{-1/2}$, which agrees with the experimental findings in Refs. [6,7]. The decay rate criterion [32] $\dot{\gamma} \simeq \Gamma_b$ is equivalent to set $C_s = 1$. At large shear rates to approach $\dot{\gamma}_{\max}$, N^* does not scale so strictly. The curves flatten out near the origin. This arises because the size preferred by the baroclinic modes is too close to the MLV core size λ. Interestingly, the experimental data in figure 11 of Ref. [7] also show similar behavior.

From Eq. (12), the MLV diameter $D = 2N^*d$ becomes

$$D \simeq 1.8(\lambda/d)^{1/4}\sqrt{\mu\bar{B}}\dot{\gamma}^{-1/2} = S\dot{\gamma}^{-1/2} \tag{13}$$

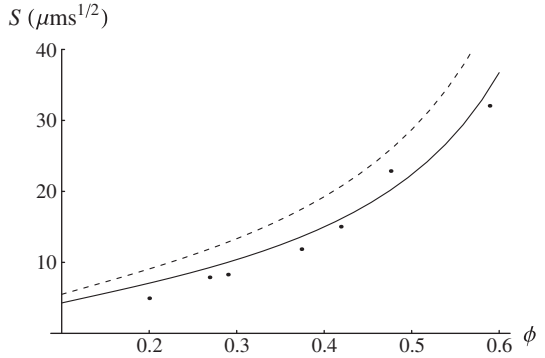

FIG. 4. The slope S in Eq. (13) at different volume fractions. The solid line is a fit with $\lambda/d = 0.7$. The dashed line is for $\lambda/d = 1.9$. The data are redrawn from figure 30(a) of Ref. [7].

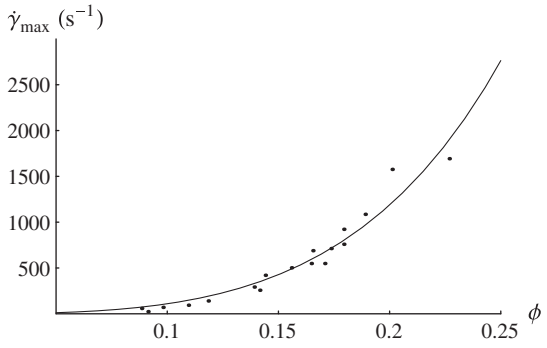

FIG. 5. The phase boundary Eq. (15) with $\lambda/d = 1.9$. The data is redrawn from figure 4 of Ref. [7].

Our calculation for μ does not consider the finite bilayer thickness δ. Using a better expression [26] $\mu = (d-\delta)^2/12\eta$, and

$$\bar{B} = \frac{9\pi^2}{64}\frac{(k_B T)^2}{\kappa}\frac{d}{(d-\delta)^4}, \tag{14}$$

one obtains $S \propto k_B T(\kappa\eta)^{-1/2}(\lambda d)^{1/4}/(d-\delta)$. Here, in Fig. 4, we plot S using a fit to the measured data [26] $\mu\bar{B} \simeq 5.18 \times 10^{-11}\phi^{-1}(1/\phi - 1.25)^{-2}$ $m^2\,sec^{-1}$, where $\phi \simeq 2.4$ nm$/d$ is used to convert d to ϕ. In the dilute lamellar, we recover the theoretical scaling $S \propto d^{-1/2}$ in Ref. [7] (assuming $\lambda \propto d$). At high concentrations, however, the measured $\mu\bar{B}$ increases much faster than $d^{-1/2}$. We find that S correlates well with the measured $\mu\bar{B}$.

The terminal shear rate ratio $\dot{\gamma}_{max}/\gamma_0$ depends on the parameter λ/d. Between $0.125 \le \lambda/d \le 4$, within an error of 10%, we find that $\dot{\gamma}_0/\dot{\gamma}_{max} = 172(\lambda/d)^2$; alternatively,

$$\dot{\gamma}_{max} = \frac{6\mu\bar{B}}{(13.1\lambda)^2} \tag{15}$$

In Fig. 5, we show the experimental phase boundary between the MLV phase and the MLV-lamellar coexisting region from Ref. [7]. Equation (15) fits the phase boundary well with $\lambda/d = 1.9$. The same value of λ/d, however, predicts a larger MLV size (dashed line in Fig. 4). Nevertheless, it is significant that the dynamic phase boundary can be obtained from the equilibrium parameters λ and $\mu\bar{B}$. The phase boundary is calculated here from MLV stability, whereas Ref. [17] discussed the problem from the point of (albeit single component) lamellar stability. A fuller analysis should include both approaches.

In summary, we calculate the baroclinic mode dispersion of a MLV. With the affine applied shear, the dynamic free energy density shows a minima for shear rates below a maxima shear rate [see Eq. (15)]. The local minima selects the steady shear MLV size, Eq. (13). Given the equilibrium parameters $\mu\bar{B}$ and λ/d, our predictions compare reasonable well with the experiments.

The support from the National Science Council and the National Taiwan University is acknowledged.

*cydlu@ntu.edu.tw

[1] F. Gauffre and D. Roux, Langmuir **15**, 3738 (1999).
[2] B. E. Cohen, Biochim. Biophys. Acta **857**, 117 (1986).
[3] S. Segota and D. Tezak, Adv. Colloid Interface Sci. **121**, 51 (2006).
[4] L. Ramos, D. Roux, P. D. Olmsted, and M. E. Cates, Europhys. Lett. **66**, 888 (2004).
[5] L. Saunders, J. Perrin, and D. Gammack, J. Pharm. Pharmacol. **14**, 567 (1962).
[6] D. Roux, F. Nallet, and O. Diat, Europhys. Lett. **24**, 53 (1993).
[7] O. Diat, D. Roux, and F. Nallet, J. Phys. II (France) **3**, 1427 (1993).
[8] T. D. Le, U. Olsson, K. Mortensen, J. Zipfel, and W. Richtering, Langmuir **17**, 999 (2001).
[9] H. Hoffmann, U. Munkert, C. Thunig, and M. Valiente, J. Colloid Interface Sci. **163**, 217 (1994).
[10] A. Leon, D. Bonn, J. Meunier, A. Al-Kahwaji, O. Greffier, and H. Kellay, Phys. Rev. Lett. **84**, 1335 (2000).
[11] W. Richtering, Curr. Opin. Colloid Interface Sci. **6**, 446 (2001).
[12] J. Penfold, E. J. Staples, A. K. Lodhi, I. Tucker, and G. J. T. Tiddy, J. Phys. Chem. B **101**, 66 (1997).
[13] J. Zipfel, P. Lindner, M. Tsianou, P. Alexandridis, and W. Richtering, Langmuir **15**, 2599 (1999).
[14] A. G. Zilman and R. Granek, Eur. Phys. J. B **11**, 593 (1999).
[15] G. K. Auernhammer, H. R. Brand, and H. Pleiner, Rheol. Acta **39**, 215 (2000).
[16] S. W. Marlow and P. D. Olmsted, Eur. Phys. J. E **8**, 485 (2002).
[17] A. S. Wunenburger, A. Colin, T. Colin, and D. Roux, Eur. Phys. J. E **2**, 277 (2000).
[18] L. Courbin, J. P. Delville, J. Rouch, and P. Panizza, Phys. Rev. Lett. **89**, 148305 (2002).
[19] F. Nettesheim, J. Zipfel, U. Olsson, F. Renth, P. Lindner, and W. Richtering, Langmuir **19**, 3603 (2003).
[20] G. I. Taylor, Proc. R. Soc. A **146**, 501 (1934).
[21] E. van der Linden, W. T. Hogervorst, and H. N. W. Lekkerkerker, Langmuir **12**, 3127 (1996).
[22] J. Bergenholtz and N. J. Wagner, Langmuir **12**, 3122 (1996).
[23] L. Courbin, G. Cristobal, J. Rouch, and P. Panizza, Europhys. Lett. **55**, 880 (2001).
[24] E. van der Linden and J. H. M. Droge, Physica (Amsterdam) **193A**, 439 (1993).
[25] Y. Kosaka, M. Ito, Y. Kawabata, and T. Kato, Langmuir **26**, 3835 (2010).
[26] F. Nallet, D. Roux, and J. Prost, J. Phys. II (France) **50**, 3147 (1989).
[27] F. Brochard and P.-G. de Gennes, Pramana Suppl. **1**, 1 (1975).
[28] S. Ramaswamy, J. Prost, W. Cai, and T. C. Lubensky, Europhys. Lett. **23**, 271 (1993).
[29] W. Helfrich, in *Liquid at Interfaces, Les Houches XLVIII (1988)*, edited by J. Charvolin, J. F. Joanny and J. Zinn-Justin (North-Holland, Amsterdam, 1990).
[30] T. C. Lubensky, J. Prost, and S. Ramaswamy, J. Phys. II (France) **51**, 933 (1990).
[31] G. Sigaud, C. W. Garland, H. T. Nguyen, D. Roux, and S. T. Milner, J. Phys. II (France) **3**, 1343 (1993).
[32] P. Panizza, D. Roux, V. Vuillaume, C.-Y. D. Lu, and M. E. Cates, Langmuir **12**, 248 (1996).